Catal Lett (2008) 121:226–233
DOI 10.1007/s10562-007-9319-y

Structure Sensitivity of Nano-structured CdS/SBA-15 Containing Au and Pt Co-catalysts for the Photocatalytic Splitting of Water

Puja S. Lunawat · Rajiv Kumar · Narendra M. Gupta

Received: 3 October 2007 / Accepted: 16 October 2007 / Published online: 2 November 2007

Abstract Photocatalysts containing nanocrystallites of cadmium sulphide dispersed in the channels of mesoporous silicate SBA-15 exhibited enhanced activity for visible-light mediated splitting of water, as compared to bulk CdS. Whereas the incorporation of 1 wt.% Pt co-catalyst in CdS/SBA-15 led to a substantial increase in H_2 yield, Au at similar loading resulted in marginally decreased activity. The results indicate that the photocatalytic activity of CdS crystallites is structure sensitive. Similarly, the role of a noble metal may be associated with the particle size dependent micro-structural features, rather than its electronic properties such as the work function or the heat of adsorption of reactant or product molecules.

Keywords Nano-structured cadmium sulphide · Photocatalysis · Structure sensitivity · Splitting of water · Role of noble metal co-catalyst

1 Introduction

The large scale production of hydrogen by means of semiconductor mediated photocatalytic splitting of water remains an un-fulfilled dream as yet, even after more than three decades of the discovery of this process by Fujishima and Honda [1]. The main limitations in the commercial exploitation of this process pertain to the low quantum efficiency, difficulty in the recovery of a photocatalyst when dispersed in water, and the loss of its activity over a period of time. With a view to overcome these constraints, concerted efforts have been devoted during last few years to prepare various nano-structured semiconducting materials, so as to improve their surface-to-volume ratio and hence the reaction efficiency, as is reviewed in several articles [2, 3]. Another approach has been to confine these nano-particles in certain porous silicate matrices in order to ensure easier catalyst recovery after completion of the reaction and at the same time to provide a hydrophobic environment to catalyst particles [4–12]. We have reported recently that the CdS nanocrystallites anchored over certain water-repellent polymeric surface not only exhibit a high catalytic activity for visible light-driven hydrogen production from water splitting, they also maintain a significantly long active life because of the hydrophobic nature of the support [13]. We now report on the photocatalytic properties of CdS nanocrystallites deposited in zeolite SBA-15 at the loadings of 2.5–10 wt.%. This particular silica support was chosen because of its hydrophobic nature, comparatively high chemical and hydrothermal stability, and at the same time one-dimensional large-size cylindrical pores of SBA-15. Corresponding CdS/SBA-15 composite catalysts incorporating highly dispersed Au or Pt metal were also synthesized in order to understand the promotional role played by a noble metal in the semiconductor-mediated photocatalytic processes, as is reported in earlier studies [14]. The samples were characterized for physico-chemical properties and their photocatalytic activity was monitored for the visible-light induced splitting of water. Another study on SBA supported CdS photocatalyst for such an application has been reported recently by Hirai et al. [15]. 2-propanol was employed as a sacrificial agent, as the addition of certain electron donor chemicals is known to augment the rate of hydrogen release [14, 15].

P. S. Lunawat · R. Kumar · N. M. Gupta (✉)
Catalysis Division, National Chemical laboratory, Pune 411008, India
e-mail: nmgupta@ncl.res.in

2 Experimental Methods

2.1 Catalyst Preparation

The SBA-15 host was synthesized using tetraethyl orthosilicate (TEOS) as a silica source and Pluronic P123 (Aldrich) as a structure directing agent. Following an earlier reported procedure [16], the silicate gel of appropriate molar composition was aged at 35 °C for a period of ~24 h under constant stirring followed by a hydrothermal treatment at 80 °C for 15 h. The recovered solid product was washed and dried in air at room temperature. After raising the temperature at 1° per minute, the sample was calcined at 500 °C for about 6 h. For the loading of CdS, an aliquot of SBA-15 was soaked with desired amount of cadmium acetate (Loba chemicals) dissolved in methanol, accompanied with constant stirring and followed by exposure to H_2S flow. After filtration, the sample was dried at room temperature and then heated at 200 °C. The samples were prepared with CdS loadings of ca. 2.5, 5 and 10 wt.% and are denoted as CdS(x)/S in the text, where x represents the loading in weight percent and S stands for SBA-15 host matrix. Taking CdS(5)/S as a representative starting material, composite catalysts containing 1 wt.% of either Au or Pt were synthesized in a small two-neck round bottom flask fitted with a reflux condenser. A method reported by Lin et al. [17] was adopted for this purpose, where H_2PtCl_6 or $HAuCl_4$, solutions in methanol were employed as metal precursor and sodium citrate as capping agent. The sodium citrate and metal salt (about 3:1 molar ratio) in methanol solution were refluxed at 353 K under stirring. The reaction was allowed for ~30 min, when the solution turned black in case of Pt and purple for Au, and the flask was then immersed in chilled water. This solution was then contacted with CdS (5%)/S for ~30 min under stirring, followed by evaporation on a rotavapor. Samples, dried initially at room temperature and then at 200 °C, are denoted in text as Pt/CdS/S and Au/CdS/S.

2.2 Photocatalytic Activity

Hydrogen evolution as a result of water splitting was monitored in a quartz reaction cell, with a provision of withdrawal of samples at regular intervals. 0.1 g of catalyst was taken in 20 mL of water to which 15 vol.% 2-propanol was added [15]. A 500 W Halogen lamp (Philips, India) surrounded by flowing water channel of ~0.5 cm width to cut-off heat radiation, was employed as radiation source. The reaction cell was held vertically at a distance of ~3 cm from the lamp. The hydrogen evolved was analyzed periodically by using a gas chromatograph (Shimatzu, model 15 A), equipped with a molecular sieve-5A packed column and a thermal conductivity detector maintained at 355 K. No attempt was made to monitor the other reaction product O_2.

2.3 Characterization

X-ray powder diffraction (XRD) patterns were taken at a scan rate of 1 min^{-1} on Rigaku (Miniflex, Japan) diffractometer using CuKα (1.5406 A°) radiation. The UV–visible spectra were recorded on Perkin Elmer spectrophotometer in spectral range 200–800 nm, using barium sulphate as reference. The information about CdS crystallite size was obtained by using transmission electron microscopy (TEM) and a JEOL 1200 EX instrument was employed for this purpose. The samples were dispersed in isopropanol for transferring them to a copper grid. The specific surface area and pore size were analyzed on Quantachrome model-NOVA 1200 equipment. The samples were evacuated at 473 K prior to N_2 sorption at 77 K. The specific surface area (S_{BET}) was calculated from the linear part of BET (Brunauer–Emmet–Teller) plots while the method of Barret–Joyner–Halenda (BJH) was used to determine the pore size distribution.

3 Results and Discussion

3.1 Physical Characteristics

The nitrogen adsorption/desorption isotherms of calcined SBA-15 and also of the CdS loaded samples were of type-IV showing H1 hysterisis loop, a typical feature of the mesoporous silicates. The surface area, pore diameter and pore volume of different samples, as derived from N_2-adsorption data, are reported in Table1. A marginal decrease in the surface area and the pore size of the photocatalysts may be attributed to ingress of CdS, Au or Pt particles in the channels of the host matrix, as confirmed by electron microscopy results. The scanning electron microscopy pictures revealed that the as-synthesized SBA-15 was of rod like morphology (not shown). Transmission electron microscopy (TEM) images showed a well ordered hexagonal array of mesopores in all the samples, a well reported feature of SBA zeolite. The average diameter of these pores was found to be ~6 nm, matching well with the N_2-adsorption data (Table 1). Very few individual CdS crystallites were seen in the TEM micrographs of CdS (2.5)/S (Fig. 1a), while they were more abundant in the samples having higher loadings (Fig. 1b, c). The size of the CdS crystallites, seen as randomly distributed round size dark objects covering the pore openings in Fig. 1b, c, was found to vary in the range 2–6 nm. The TEM results also

Table 1 Physical characteristics of SBA-15 and CdS loaded photocatalysts

No.	Photocatalyst	Surface area (S_{BET}) ($m^2\ g^{-1}$)	Pore volume ($cm^3\ g^{-1}$)	Pore diameter (D_{BJH}) nm	Average CdS crystallite size[a] (nm)
1	SBA-15	733	1.00	6.7	–
2	CdS(2.5)/S	667	0.90	6.7	Not measurable
3	CdS(5)/S	626	0.83	5.7	4.5
4	CdS(10)/S	616	0.81	5.7	7.5
5	Pt/CdS(5)/S	598	0.80	6.7	–
6	Au/CdS(5)/S	610	0.81	6.7	–
7	CdS powder	–	–	–	17.0

[a] From XRD data

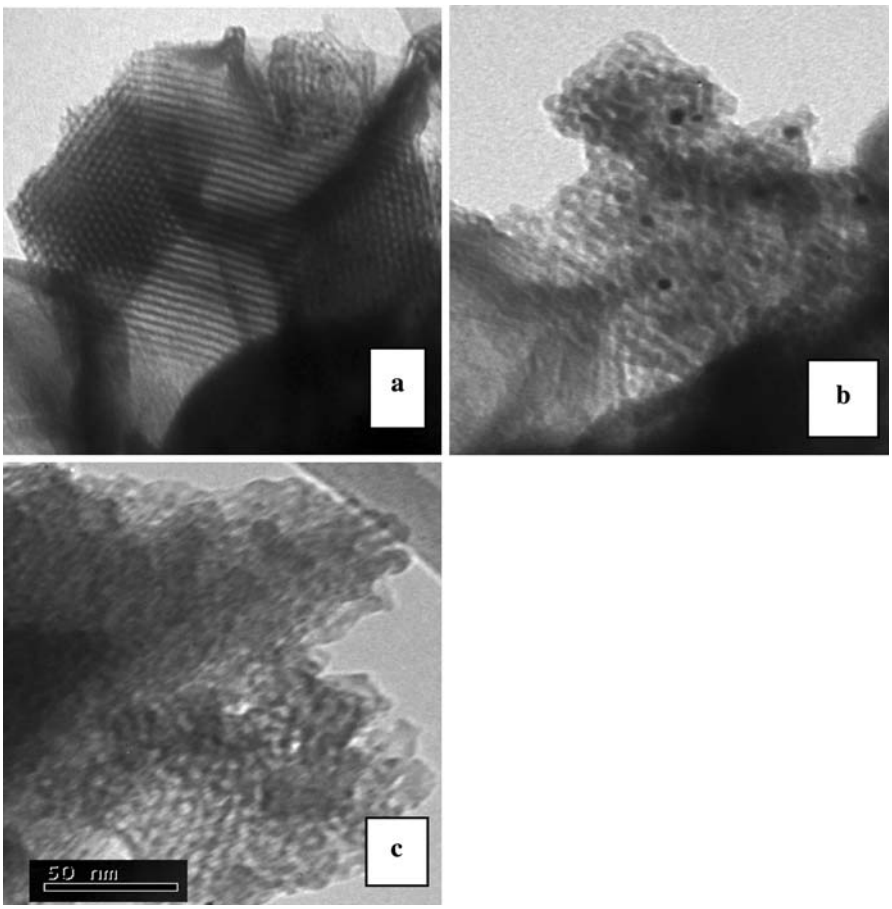

Fig. 1 Transmission electron micrographs of (**a**) CdS(2.5)/S, (**b**) CdS (5)/S, and (**c**) CdS (10)/S samples

reveal that the incorporation of CdS has no significant effect on the original mesopore structure of SBA-15.

3.2 XRD

The powder X-ray diffraction (XRD) patterns of base material SBA-15 (curve a, Fig. 2) showed a prominent low angle reflection at $2\theta = 0.95°$ along with two low intensity lines at ca. 1.65 and 1.9°, which match well with the characteristic (100), (110) and (200) reflections of mesoporous SBA-15 having p*6* mm symmetry (16). Curves b–f in this figure show the XRD reflections of CdS loaded SBA samples, and also their Au and Pt containing nano-composites. These data clearly reveal that the structure of the host matrix remained unaffected after inclusion of the CdS or the co-catalyst particles.

Curves a–d in Fig. 3 exhibit the XRD patterns of SBA samples in 2θ range 10–70°, without and for different loadings of CdS. Curve (e) shows the XRD reflections of a bulk CdS sample, synthesized by precipitation from a methanol solution of cadmium acetate, followed by filtration, drying, and heating in N_2 at 500 °C. The XRD lines marked * in Fig. 3 (curve e) and appearing at 2θ values of 26.7, 30.9, 44.0 and 52.0° are the characteristic reflections of cubic (β) phase of CdS (JSPD S01-0647). Several low intensity XRD lines in

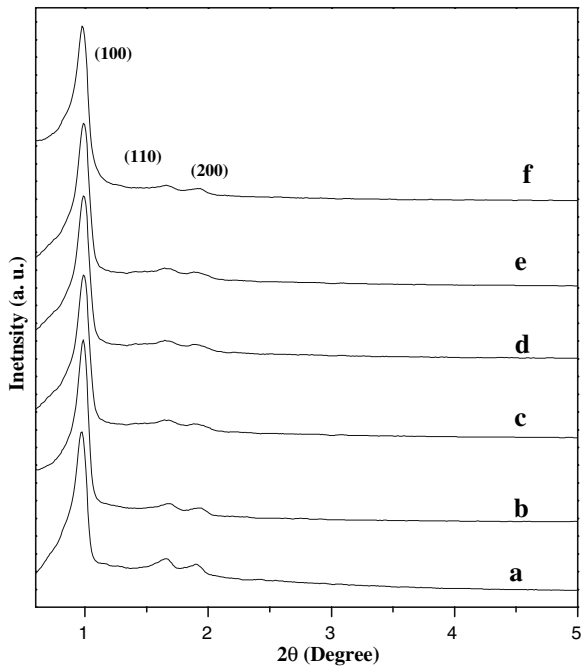

Fig. 2 Low angle powder X ray diffraction patterns of (a) SBA-15 with no loading, (b) CdS(2.5)/S, (c) CdS (5)/S, (d) Pt/CdS (5)/S, (e) Au/CdS (5)/S, and (f) CdS (10)/S samples

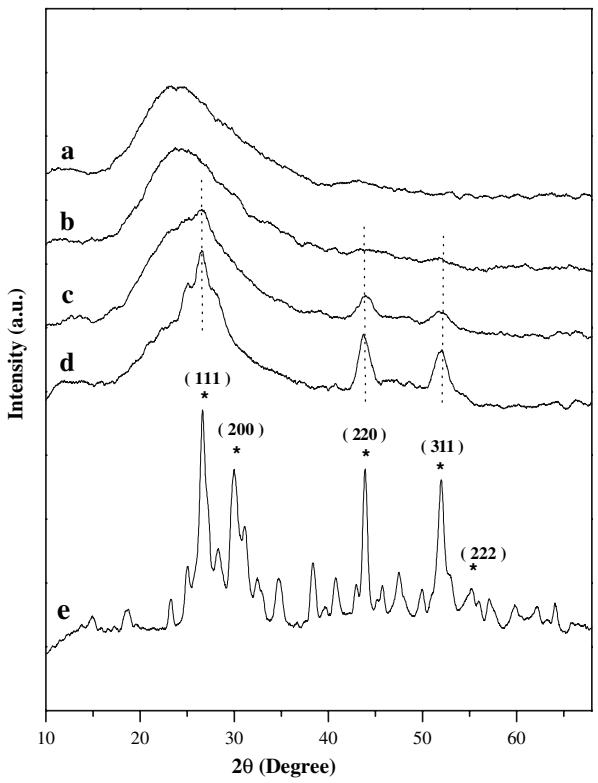

Fig. 3 Wide angle powder X ray diffraction patterns of (a) SBA-15, (b) CdS(2.5)/S, (c) CdS (5)/S, (d) CdS (10)/S, and (e) bulk CdS samples

this figure arise due to hexagonal (α) phase of CdS. Data in Fig. 1b–d thus reveal that the CdS particles in SBA-15 exist mainly in the *β*-phase. Considerable line broadening observed in curves (b–d) is a characteristic feature associated with small (nanosize) crystallites. The average size of CdS particles, estimated by using Debye-Sherrer formula, is found to be around 17, 8 and 4.6 nm in bulk CdS, CdS(10)/S and CdS(5)/S samples, respectively. The further broadening of XRD lines in Fig. 1b suggests that the CdS particles in the sample containing 2.5 wt.% loading were of size smaller than 3–4 nm, which is the detection limit of XRD measurement. These results clearly reveal that the crystallite size increases progressively with increase in CdS loading, as was observed in our earlier study also [13]. Furthermore, similar XRD patterns were observed for Pt/CdS/S and Au/CdS/S samples also, revealing the structural integrity of the composite catalysts as well. No individual reflections due to Au or Pt were detected in the XRD patterns of these samples, indicating again the high dispersion and the nano-size of the metal particles.

3.3 UV–Visible Spectra

Figure 4 exhibits the diffuse-reflectance UV–visible absorption spectra of different CdS/S and bulk CdS samples. The decrease observed in the absorbance of SBA-15

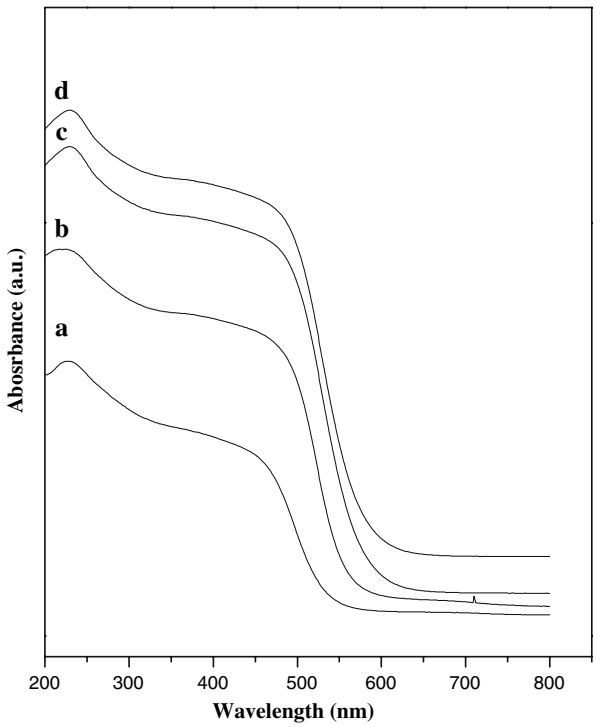

Fig. 4 DR UV–visible absorbance spectra of (a) CdS(2.5)/S, (b) CdS (5)/S, (c) CdS (10)/S, and (d) bulk CdS samples

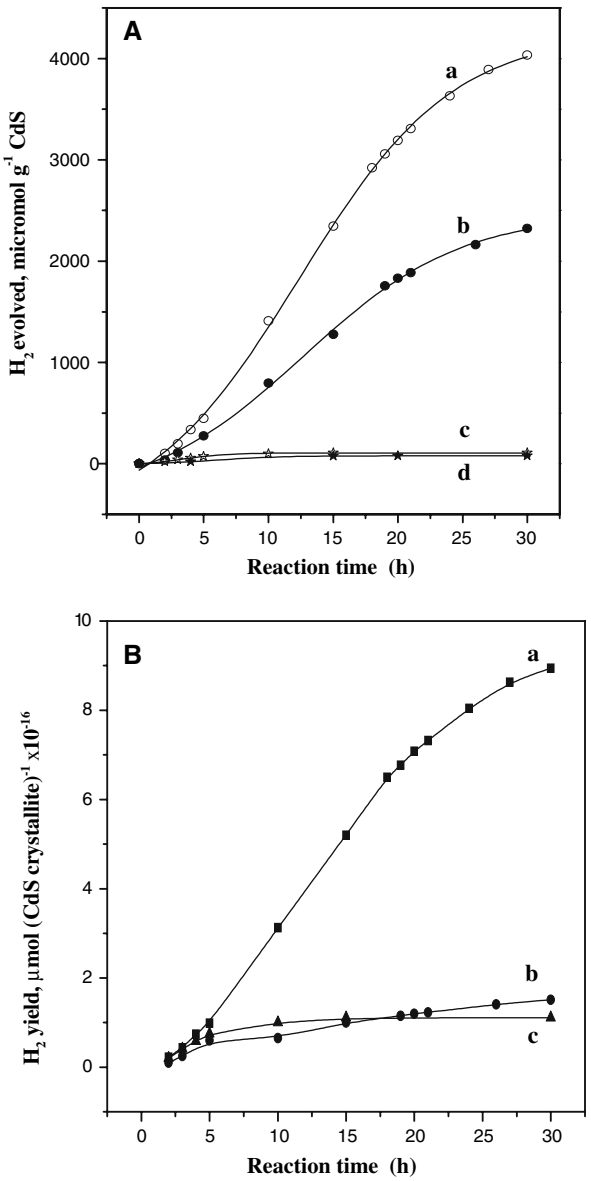

Fig. 5 (**A**)-Hydrogen evolved g^{-1} of CdS during photocatalytic splitting of water over (a) CdS (5)/S, (b) CdS(2.5)/S, (c) CdS (10)/S, (d) bulk CdS. (**B**)-Specific activity of (a) CdS(5)/S, (b) CdS(2.5)/S and (c) CdS (10)/S for photocatalytic splitting of water

supported catalysts is commensurate with the amount of CdS available in a particular sample. We also observe a progressive shift in the onset of absorption edge to lower wavelength region (curves a–c), which finds a correlation with the loading-dependent decrease in CdS particle size. This feature may be ascribed to the well-reported quantum-confinement effect [18].

3.4 Photocatalytic Activity

The formation of H_2 commenced within ~15 min time, when the catalytic reactor containing suspension of a CdS/S sample in water-propanol (15 vol.%) mixture was exposed to visible light, and the brisk formation of H_2 bubbles continued till about 70 h of a typical test runs without any apparent decrease in hydrogen yield. No reaction was observed under dark condition. Curves a–c in Fig. 5A depict the time dependent progress of photocatalytic reaction for the samples containing different loadings of CdS. Curve (d) in this figure shows comparative catalytic activity of a powder CdS sample. As seen in this figure, the amount of hydrogen evolved per unit mass of CdS in a sample follows a trend: CdS(5)/S > CdS(2.5)/S > CdS(10)/S > Bulk CdS. Taking into account the size of CdS particles in different samples (Table 1), the activity results clearly indicate an important role of the dispersion and the size of the CdS particles, in addition to the amount of photocatalyst loaded in a sample. In general, smaller is the size of CdS particles better is the catalyst performance because of the increase in surface to volume ratio of active catalyst component (curve a, Fig. 5a).

In order to further highlight the dispersion effect, the specific activity of three CdS/S samples, i.e., the yield of H_2 per unit CdS particle, are plotted in Fig. 5b. The number of CdS particles available in a particular sample was estimated on the basis of the crystallite size data (Table 1), assuming the shape of each particle to be spherical. These results further illustrate that the particle size plays a crucial role in determining the photocatalytic activity of a semiconducting material. This particle size effect is similar to the structure-activity relationships observed in the case of several noble metal catalysts. For instance, although bulk gold is known to be a poor catalyst for CO oxidation, around ~3 nm size Au crystallites are found to exhibit the highest activity in case of Au/TiO_2 catalysts [19, 20]. Not only the noble metals, the chemical properties of semiconductor nano-crystals are also reported to be size-dependent [21]. Various explanations have been offered for these size-specific properties of the nano-structured particles, such as modification of electronic structure and varying surface properties at metal/support interfaces as a function of crystallite size [20, 21]. It is therefore suggested that the activity trend seen in Fig. 5b may have its origin in the structure sensitivity of CdS photocatalyst, the presence of the micro-structural surface defects playing an important role. The strong bonding of molecules at rough single crystal surfaces comprising of certain structural defect centers and the unique catalytic activity of oxide–metal interfaces have indeed been demonstrated [22].

In order to assess the long term stability of SBA supported samples, the activity of a representative CdS(5)/S photocatalyst was monitored over a period of several days for splitting of water under visible light. Figure 6 presents these results where the experiment was interrupted after about 30 h of an initial test run (curve a). The sample was

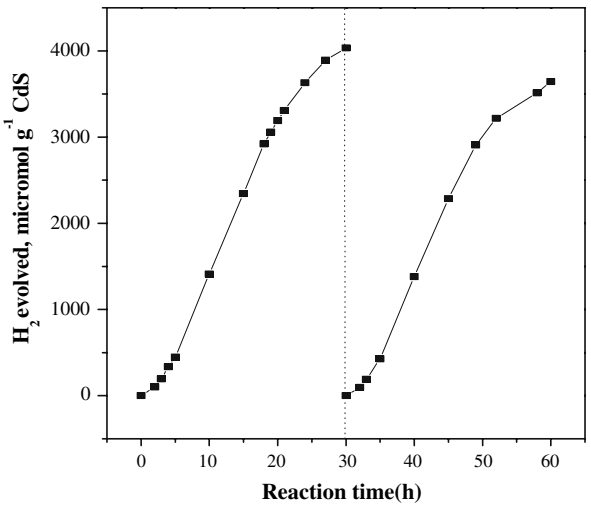

Fig. 6 Amount of hydrogen evolved g^{-1} of CdS during the two successive cycles (30 h each) of photocatalytic splitting of water over CdS(5)/S, with in between interruption and flushing with nitrogen

then flushed with nitrogen and was reused for the next cycle of 30 h experiment (curve b). As seen in Fig. 6a, b, a similar rate of hydrogen evolution is observed during these two reaction cycles. Similar trend was observed when such experiments with in-between breaks were repeated several times. The XRD pattern recorded on the sample recovered after this prolonged contact with water revealed its structural stability.

Figure 7 depicts the hydrogen yield during photocatalytic splitting of water using samples Pt/CdS(5)/S (curve a), CdS(5)/S (curve b) and Au/CdS(5)/S (curve c), containing identical loadings at 5 wt.% of CdS and 1 wt.% of Au or Pt. As seen in curve Fig. 7a, the photocatalytic activity of CdS is found to increase substantially by inclusion of Pt. On the other hand, almost no change in catalytic activity was observed in the case of CdS/S sample containing a similar amount of gold, besides a small decrease in hydrogen yield (Fig. 7c).

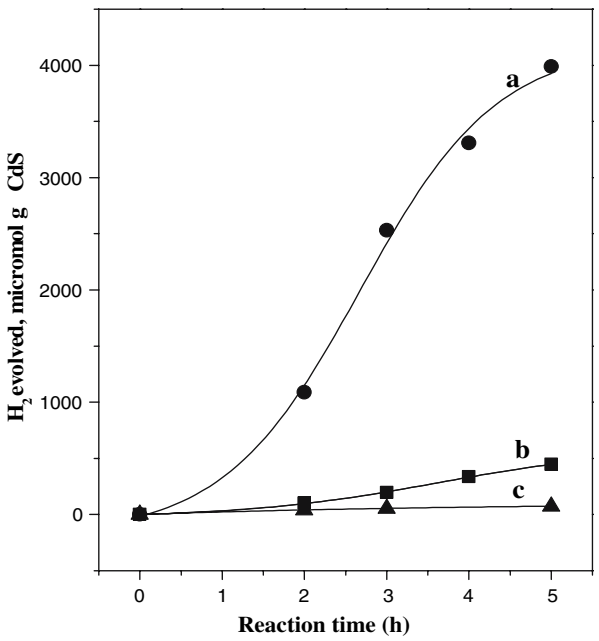

Fig. 7 Comparative amounts of hydrogen evolved g^{-1} of CdS during the photocatalytic splitting of water over (a) Pt/CdS(5)/S, (b) CdS (5)/S, and (c) Au/CdS(5)/S samples

The role of a co-catalyst in semiconducting materials has been debated extensively and many contradictory explanations have been offered for the noble metal induced enhancement of photocatalytic activity, both for the splitting of water and for the mineralization of volatile organic contaminants. According to one school of thought, a noble metal serves as electron sink to minimize the recombination of photo-generated charge carriers, leading thereby to improved quantum efficiency [23–25]. Another explanation envisages a correlation between the enhanced photocatalytic activity and the work function of the deposited co-catalyst [26]. While discounting such a relationship, Subramanian et al. [27], on the other hand, proposed that the deposition of the organic-capped noble metal particles of Au, Pt and Ir on nano-structured TiO_2 film cause a shift in the quasi-Fermi level of the composite, resulting in the decreased over-voltage of interfacial charge transfer process. The extent of this energy level shift is found to be dependent of the particle size of the noble metal. In a recent study on visible light induced photocatalytic splitting of water over platinum group metals dispersed on CdS nanocrystallites, Satish et al. [28] proposed that the rate of hydrogen production can be related to the metal-hydrogen bonding, and the electron work function and redox potential of the noble metal atom. These authors suggested that the better performance of Pt as a co-catalyst compared to other platinum group elements such as Pd, Rh and Ru can be ascribed to its higher work function, lower metal-hydrogen bond energy, and more positive redox potential. It was argued that when the metal-hydrogen bond energy is less, the hydrogen evolution barrier is substantially reduced, resulting in easy evolution of molecular hydrogen. Similarly, more positive is the redox potential of the noble metal the faster will be the reduction of H^+ ions generated during H_2O–h^+ interaction [28].

We, however, observe that many of the above-mentioned correlations may not hold good when we take into account the physical–chemical properties of Pt and Au metals (Table 2) and the activity data presented in Fig. 7. For instance, whereas electron work function of the two metals is quite comparable, the reduction potential of Au is considerably higher than that of Pt. Similarly, since the heat of hydrogen adsorption is at least three times lower

Table 2 Comparison of some physical–chemical properties of polycrystalline platinum and gold metals

Metal	Electron work function[a] (ϕ), eV	ΔH_{ads} H_2^b kcal mol^{-1}	ΔH_{ads} O_2^b kcal mol^{-1}	ΔH_{ads} H_2O^c kcal mol^{-1}	Reduction potential[d] E^o, V
Pt	5.64	25–30	70	16.4	+1.18
Au	5.4	8–10	40	15.5	+1.692

[a] Ref. [31]

[b] Ref. [32]

[c] Ref. [33]

[d] Standard reduction potential for reactions $Pt^{2+} + 2e \rightleftarrows Pt$, and $Au^{+} + e \rightleftarrows Au$, from Ref. [31] in footnote (a)—pp 8–23

on Au as compared to Pt, one would expect much higher catalytic activity with Au co-catalyst, in contrast to the results shown in Fig. 7c. It is therefore apparent that the surface properties and not the electronic structure of a highly dispersed metal co-catalyst may play a vital role, an aspect not given a serious thought so far. The activity trend in Fig. 7 is in fact commensurate with the well-reported size-dependence of the catalytic properties of metals. The structure-sensitivity of small (nanosize) noble metal particles, including Au and Pt, is known to make them active for certain reactions and at the same time inactive for others [20, 29, 30]. By similar analogy, it can be argued that the metal–CdS interfaces in composite photocatalyst may promote the adsorption of water molecules, thus enhancing their interaction with the photo-generated charge carriers. Just as an optimum size of Au or Pt particles is a prerequisite for certain catalytic processes, such as adsorption and oxidation of CO [19], it is imperative that the adsorption of water molecules is also structure-sensitive. An optimum crystallite size of semiconductor and metal component may thus promote the photocatalytic processes involved in the dissociation of water. It is likely that this optimum size may vary for different photocatalytic materials and also for different noble metals, thus explaining the results in Figs. 5and 7. In fact, an over-size metal particle may result in decrease in the activity by covering some of the active semiconductor sites, as seen in the results of Fig. 7c.

4 Conclusions

In conclusion, the results of our study reveal that both the semiconductor and the dispersed metal phase in a composite photocatalysts may exhibit structure-sensitivity for the adsorption of water molecules. The size-tuning of both the components may therefore prove to be vital for synthesizing an efficient photocatalyst for splitting of water. More detailed experiments are now planned to further substantiate these ideas.

Acknowledgment NMG thanks CSIR for a research grant under the Emeritus Scientist scheme. Authors thank Mr. Mahesh Kadgaonkar for helping in manuscript preparation.

References

1. Fujishima A, Honda K (1972) Nature (London) 238:37
2. Beydoun D, Amal R, Low G, McEvoy S, (1999) J Nanopart Res 1:439
3. Chen X, Mao S (2007) Chem Rev 107:2891
4. Xu Y, Langford CH (1995) J Phys Chem 99:11501
5. Hsien Y–H, Chang C-F, Cheng Y–H, Cheng S (2001) Appl Catal B: Environ 31:241
6. Reddy EP, Davydov L, Smirniotis PG (2002) J Phys Chem B 106:3394
7. Gies H, Grabowski S, Bandyopadhyay M, Grunert W, Tkachenko OP, Klementiev KV, Birkner A (2003) Micropor Mesopor Mater 60:31
8. Adams WA, Bakker MG, Macias T, Jefcoat IA (2004) J Hazardous Mater B112:253
9. López-Muñoz M-J, van Grieken R, Aguado J, Marugán J (2005) Catal Today 101:307
10. Bhattacharya K, Tripathi AK, Dey GK, Gupta NM (2005) J Nanosci Nanotechnol 5:790
11. Bhattacharya K, Varma S, Kumar D, Gupta NM (2005) J Nanosci Nanotechnol 5:797
12. Kumar D, Gupta NM (2005) Catal Surv Asia 9:35
13. Lunawat PS, Senapati S, Kumar R, Gupta NM (2007) Int J Hydrogen Energy 32:2784
14. Kiwi J, Gratzel M (1979) Nature 281:657
15. Hirai T, Nanda M, Komasawa I (2003) J. Colloid Interface Sci 268:394
16. Zhao D, Huo Q, Feng J, Chmelka B, Stucky G (1998) J Am Chem Soc 120:6024
17. Lin C-S, Khan MR, Lin SD (2006) J Colloid Interface Sci 299:678
18. Kundu M, Khosravi AA, Kulkarni SK (1997) J Mater Sci 32:245
19. Choudhary TV, Goodman DW (2002) Top Catal 21:25
20. Haruta M (1997) Catal Today 36:153
21. Rao CNR, Kulkarni GU, Thomas PJ, Edwards PP (2002) Chem Eur J 8:29
22. Somorjai GA (1994) Surf Sci 299-300:849
23. Zhang Z, Wang CC, Zakaria R, Ying JY (1998) J Phys Chem B 102:10871
24. Kominami H, Muratami S, Kato J, Kera Y, Ohtani B (2002) J Phys Chem B 106:10501
25. Kamat PV, Flumiani M, Dawson A (2002) Colloids Surf A 202:269

26. Nosaka Y, Norimatsu K, Miyama H (1984) Chem Phys Lett 106:128
27. Subramanian V, Wolf E, Kamat PV (2001) J Phys Chem B 105:11439
28. Satish M, Viswanathan B, Viswanath RP (2006) Int J Hydrogen Energy 31:891
29. Bond GC, Thompson DT (2000) Gold Bull 33:41
30. Rioux RM, Song H, Hoefelmeyer JD, Yang P, Somorjai GA (2005) J Phys Chem B 109:2192
31. Lide DR (2005) CRC handbook of chemistry and physics, 85th edn. CRC Press, Boca Raton, pp 12–130
32. Toyoshima I, Somorjai GA (1979) Heat of hydrogen and oxygen adsorption. Catal Rev Sci Eng 19:105
33. Bodé DD Jr (2007) In: Hirschfelder JO, Henderson D (ed) Advances in chemical physics: chemical dynamics, vol 21. Wiley Inter Science, p 361